electronics

MDPI

Article

A Unified Active Frequency Regulating and Maximum Power Point Tracking Strategy for Photovoltaic Sources

Hongda Cai [1], Yanghong Xia [2], Pengcheng Yang [1,*], Jing Li [1], Yongzhi Zhou [2] and Wei Wei [2]

[1] School of Information and Electrical Engineering, Hangzhou City University, Hangzhou 310015, China; caihd@zucc.edu.cn (H.C.); lijing@zucc.edu.cn (J.L.)
[2] College of Electrical Engineering, Zhejiang University, Hangzhou 310027, China; royxiayh@zju.edu.cn (Y.X.); zhouyongzhi@zju.edu.cn (Y.Z.); wwei@zju.edu.cn (W.W.)
* Correspondence: ypc196@126.com

Abstract: In order to optimize the extraction of solar energy, photovoltaic sources are commonly operated under the control of the so-called maximum power point (MPPT) strategy. However, as the rate of PV installations increases explosively, traditional MPPT algorithms may cause problems such as frequency deviation and power fluctuations, making system frequency stability a challenge due to the inherent intermittent and stochastic nature of PVs. Consequently, in order to reduce the investment and maintenance costs of storage systems, innovative control is expected for PV sources to provide ancillary services for the system, especially for weak systems such as microgrids. In this paper, a novel active power control (APC) strategy, based on characteristic curve fitting, is proposed to flexibly regulate the PV output power. The transient process performance and robustness of the system are improved with the proposed APC strategy. In conjunction, an f–P droop mechanism is designed to provide a frequency regulating (FR) service for the AC microgrid. The comprehensive control strategy unifies the FR function with the traditional MPPT function in a single control structure, allowing the PV source to operate either in the MPPT mode when the system frequency is nominal or in FR mode when the frequency exceeds it. The transition between MPPT and FR is autonomous and fully decentralized, which improves the PV generation efficiency as well as ensuring generation fairness among different parallel PV sources. Importantly, the proposed control strategy does not require any internal bundled energy within the PV generation system to achieve FR capability, but it effectively collaborates with the system-level energy storage system, thus reducing the necessary battery capacity. A detailed dynamic model of a PV generation system is constructed to validate the feasibility and effectiveness of the proposed control strategy.

Keywords: frequency regulation; photovoltaic sources; AC microgrids; active power control; droop control

check for updates

Citation: Cai, H.; Xia, Y.; Yang, P.; Li, J.; Zhou, Y.; Wei, W. A Unified Active Frequency Regulating and Maximum Power Point Tracking Strategy for Photovoltaic Sources. *Electronics* **2023**, *12*, 3467. https://doi.org/10.3390/electronics12163467

Academic Editors: Ziwen Liu, Jinmu Lai and Ji Han

Received: 5 June 2023
Revised: 10 August 2023
Accepted: 14 August 2023
Published: 16 August 2023

1. Introduction

Solar energy, due to its relative low installation and maintenance costs and widespread resource distribution [1], has emerged as the predominant resource within renewable power systems. As more and more PV sources are being installed, intermittent and stochastic characteristics of irradiation are increasingly challenging and threatening to system stability control and safe operation. This problem is especially pronounced in weak systems such as AC microgrids and remote insular or mountainous power systems [2,3]. Traditionally, we use the energy storage system for frequency regulation and leave the maximum power point tracker to extract the highest available power from the PV array. As a result, PV sources do not inherently contribute to the system frequency regulation. Hence, from the perspective of the large power grid system, the projected growth of PV systems will put stress on other conventional generators and further weaken the power system stability [4]. Moreover, in future, PV systems may replace a significant part of rotational generation capacity and during favorable conditions, instantaneous penetration reaches a higher level and will result in lower system inertia. In case of any disturbance, reduced inertia may cause the problem of large frequency deviation and the rate of change of frequency (RoCoF) will be high enough to trip the generation units and activate the load-shedding controller, even at small magnitudes of load imbalance [5].

From the perspective of microgrids, with the continuous rising of PV penetration, the MPPT mode may lead to some serious problems, including but not limited to power imbalance, frequency deviation, battery overcharge and overvoltage. All these will severely threaten the safe and stable operation of the microgrids. Enlarging the system storage capacity can address the above problems, but this meanwhile increases the system installation and maintenance costs. Even if the system has sufficient energy storage capacity, there are still restrictions on charging/discharging power and the battery's SOC [6–8]. It is hard to maintain the long-term stable and reliable operation of this kind of system by relying solely on energy storage. The renewable sources such as PV should become involved.

Aside from expanding the energy storage capacity, operating the PV sources in active power control (APC) mode to provide primary FR service is a promising alternative. The authors in Ref. [9] have demonstrated that the APC exhibits superior economic benefits compared to the installation of substantial energy storage, assuming power fluctuations remain within a normal range. These findings motivate further investigations into PV sources providing active support, such as primary FR, especially in isolated or small-scaled AC microgrids with a substantial portion of installed PV capacity.

The authors in Ref. [10] introduce a control scheme that combines MPPT and DPC (delta power control). In the DPC mode, a certain amount of the PV generation is reserved to provide active support to the system. To achieve this, the PV strings' operation patterns are forced to be different, some are in MPPT mode and the others are in power reserved mode. A significant advantage of this kind of method lies in the estimation of the MPP (maximum power point) without irradiance sensors. However, this method does not ensure fair generation among PV sources. Recently, adopting proper control of the converter's DC-link capacitor to provide FR has gained increasing traction [11–13]. Despite capacitors' high efficiency and durability, their elevated cost and limited energy storage capacity constrict their applicability. In addition to exploiting DC-link capacitors, another approach involves directing PV sources to operate away from the MPP, thereby enabling participation in system FR [14–16]. Commonly, this technique involves generating an additional PV voltage deviation signal to drive MPPT reference instructions away from the MPP, thus enforcing operation of PV sources in the deloading (DL) mode. The DL control method reserves a proportion of the PV output to maintain the margin in order to respond to the frequency fluctuations and deviations. Refs. [17,18] introduce innovative dp/dv-based strategies for primary support by directly adjusting the PV output power. The V-I/V-dp/dv slopes are used for primary voltage control and multi-source cooperation. However, achieving the necessary derivative proves to be challenging, necessitating high-performance micro-controllers. The deloading control method requires continuous reservation of PV power for frequency support, leading to a wastage of solar resources. As DL algorithms demonstrate lower efficiency compared to active power control (APC), the latter has become the focus of recent research.

The primary challenge in applying the APC to a PV source lies in accurately determining the maximum power point (MPP) of the PV array. Given that each PV output power corresponds to two distinct operating points, with the exception of the MPP, designing a stable power regulator for the PV source becomes complex. These operating points exhibit contradicting control characteristics, which further complicate the regulator design. Solutions generally fall into two categories: MPP searching schemes and MPP estimation methods. For the former, Ref. [19] proposes a reference power tracking strategy, utilizing a mode detection and switching module to decide the PV operating point and, accordingly, switch between the appropriate voltage regulators. This solution is straightforward, but the transition impact during the regulator switching might impair the performance. Ref. [20]

puts forward a universal controller consisting of a fast MPPT (FMPPT) controller and a slow MPPT (SMPPT) controller. The transition between controllers may not be seamless, potentially affecting system stability and inducing unwanted oscillations. A novel Newton quadratic interpolation-based APC algorithm is presented in Ref. [4] and utilized for system frequency regulation in Ref. [21]. The algorithm has relatively poor robustness and might cause transient problems when the irradiation or loads change rapidly and dramatically since the quadratic curve is quite different from the PV *P*–*U* curve.

To improve on methods presented in previous literature, a novel FR strategy for PV sources in AC microgrids with a traditional hierarchical control framework is introduced in this paper. With the proposed strategy, PV sources can either provide FR service when necessary or operate in MPPT mode to absorb as much of the solar resource as possible. The PV sources adaptively deliver primary FR control based on the system frequency deviation, and its FR capability naturally adjusts with irradiation variations. The proposed scheme unifies MPPT and FR within a single controller, eliminating the transition between different operating modes. Furthermore, similar to the commonly used droop control methods, it is fully decentralized and suitable for both distributed PV sources and large-scale PV plants. Importantly, the proposed control strategy does not require any internal bundled energy within the PV generation system to achieve FR capability, but it effectively collaborates with the system-level energy storage system, thus reducing the necessary battery capacity. A comparison between the proposed control strategy and the existing frequency regulation methods for PV sources is provided in Table 1.

Table 1. Frequency regulation methods for PV sources.

Frequency Regulation Methods	Main Strategy	PV-Utilization Efficiency	Generation Fairness	Unified Mode Controller	Regulation Capability	Adaptability	Strong Robustness
Ref. [8]	Delta power control	low			medium		√
Refs. [9–11]	DC-link capacitor control	high			small		√
Refs. [12–14]	Deloading control	low			large		√
Refs. [15,16]	d*p*/d*v* control	low	√	√	large		
Ref. [18]	Reference power tracking	high			large		√
Ref. [18]	FMPPT and SMPPT	high			large	√	
Refs. [19,20]	Quadratic interpolation	high	√	√	large	√	
The proposed method	Characteristic curve fitting	high	√	√	large	√	√

"√" in the table indicates that the method has the corresponding feature.

The remaining sections of this paper are organized as follows: Section 2 offers a general introduction to the proposed strategy and control structure. Section 3 elaborates on the specialized APC algorithm based on characteristic curve fitting. Section 4 examines the *P*–*f* droop control for PV sources and discusses its adaptability. Section 5 presents simulation tests, demonstrating the feasibility and effectiveness of the proposed strategy through the results. Finally, Section 6 concludes the paper.

2. Principles of the Proposed Control Strategy

The main features of the proposed PV control strategy are as follows:

(1) The PV works in the FR mode to participate in the system frequency regulation when the system frequency surpasses its nominal value and the irradiance is sufficient. This control strategy aims to deliver frequency regulating services for the connected system, to cooperate with other synchronous sources, but not to become the sole grid-forming generator.

(2) The PV works in the MPPT mode when the system frequency is at its nominal value or the irradiance is insufficient such as shadowing time. The insufficient irradiance may lead to possible loss of FR capability of PV sources but the system is still governed by

system-level storage or other synchronous sources. Thus, the system can still work effectively at night or during shadow periods.

(3) The proposed control strategy integrates both FR mode and MPPT mode into a single APC framework, ensuring a smooth and autonomous transition between operational modes.

(4) The PV sources adapt their primary FR capability in response to system frequency deviations. Concurrently, their FR capacity adjusts based on irradiance changes, enhancing PV efficiency in contrast to conventional PV FR approaches.

(5) It is fully decentralized and suitable for both distributed PV sources and large-scale PV plants.

The concept of droop is widely utilized for FR and multiple-source cooperation in an AC microgrid, irrespective of whether it is grid-connected or islanded. Typically, the role of *P–f* type source is assumed by the energy storage and grid-connected interlink converters. Since distributed generators such as PV sources cannot participate in the primary FR such as *P–f* type sources, load changes and power fluctuations may induce significant frequency deviations. This situation becomes more problematic for weak systems such as AC microgrids that have a high portion of PV sources.

The mathematical model of the PV array current at nominal irradiance and temperature is given by [17]:

$$I_{PV} = N_P I_{sc,n} \left[1 - \exp\left(\frac{V_{PV}}{N_s a V_t} - \frac{V_{oc,n}}{a V_t} \right) \right], \tag{1}$$

where I_{PV} is the PV output current. N_P and N_s are the number of parallel- and series-connected PV modules and each module is composed of N PV cells. $I_{sc,n}$ and $V_{oc,n}$ are the short-circuit current and open-circuit voltage of the PV module at nominal condition (1000 W/m^2, 25 °C). V_{PV} is the operating voltage of the PV array and $V_t = NkT/q$ is the thermal voltage of the PV array with k being the Boltzmann constant, q being the electron charge and T being the temperature (Kelvin) of the PV cells. a is the ideality constant of the equivalent diode. The detailed explanations on PV modeling may be found in Refs. [22,23].

Then the output power of the PV array is derived from (1):

$$P_{PV} = V_{PV} I_{PV} = N_P I_{sc,n} V_{PV} \left[1 - \exp\left(\frac{V_{PV}}{N_s a V_t} - \frac{V_{oc,n}}{a V_t} \right) \right], \tag{2}$$

The nonlinear characteristic between the PV output power, P_{PV}, and its terminal voltage, V_{PV}, is illustrated in Figure 1. As shown, the *P–U* curve can be divided into two segments: (1) the uphill segment and the downhill segment, determined by the sign of $\mathrm{d}P_{PV}/\mathrm{d}V_{PV}$. Operating within these segments reveals contrasting control characteristics: the PV output increases when the PV voltage rises in the uphill segment, while it decreases in the downhill segment when the PV voltage increases. This contrast complicates the design of frequency/voltage regulators when relying solely on conventional controller adaptations. Consider a typical two-level control structure for frequency regulation, as shown in Figure 2. If an abrupt change in irradiance or system load shifts the system frequency away from its reference, and the PV sources need to reduce their output to mitigate the frequency deviation, then level 2 should modulate the PV output power according to the *P–U* curve in Figure 2. Yet, Figure 2 also indicates that the V_{PV} adjustment direction varies between the uphill and downhill segments. To decrease PV output in the uphill segment, a reduced V_{PV} is required, while the opposite is true for the downhill segment. For effective frequency regulation with linear controllers, the PV operating range must be constrained to either the uphill or downhill segments. Hence, the maximum power point, particularly the value of V_{MPP}, becomes critical for advanced PV applications such as frequency regulation.

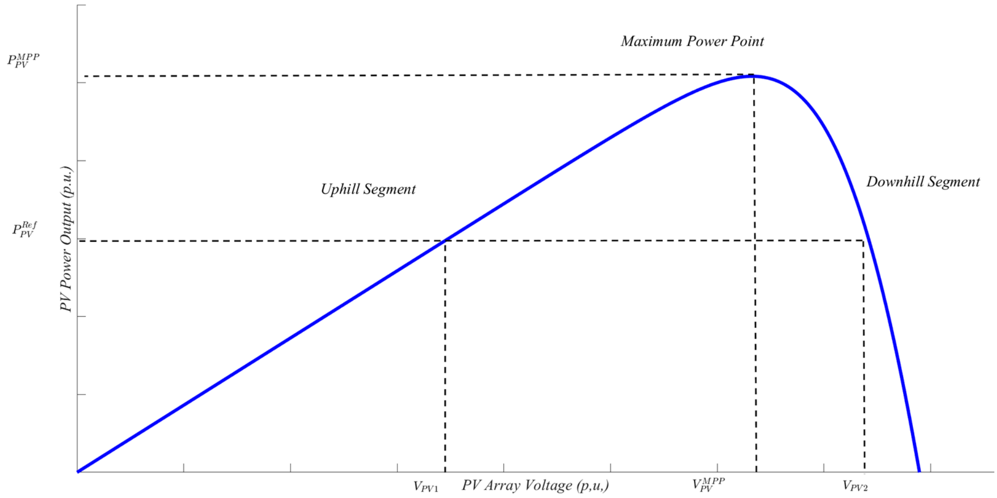

Figure 1. P–U characteristic of a typical PV source.

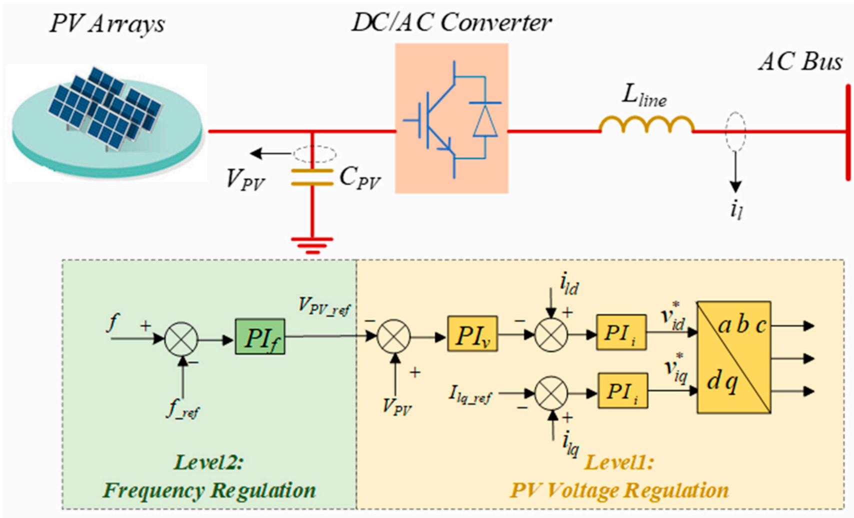

Figure 2. Two-level control structure for PV frequency regulation.

To solve the aforementioned issues, a three-level hierarchical control strategy is designed for PV sources to enable them to contribute to primary FR. Figure 3 presents the control diagram of the proposed FR strategy with a typical single-stage PV generation system. As depicted, the overall strategy comprises three control levels: PV voltage regulation (level 1), active power control (level 2) and frequency droop control (level 3).

Level 3, the outermost control loop of the proposed control strategy, primarily focuses on the FR, forming the central part of the proposed cascaded controller. A frequency droop curve is employed for PV sources to modulate their output power based on the system frequency deviation. If the system frequency is maintained within an acceptable range, PV sources will autonomously switch to the MPPT mode from FR mode. This transition is governed by the system frequency and irradiation levels, which define the FR capability of PV sources. The input to level 3 is the frequency deviation, Δf (the difference between its actual value and nominal value), and its output is the PV power reference. Essentially, level 3 determines the PV output power reference according to the system frequency deviation to provide FR service, while the inner control loops track the power references.

Level 2 identifies the accurate PV operating voltage, V_{PV}^{ref}, that corresponds with the power reference, P_{PV}^{ref}, provided by level 3, as controlling PV operating voltage is a common method for managing PV sources' output power. When P_{PV}^{ref} is less than the maximum available power point (MAPP), a V_{PV}^{ref} that corresponds to an operating point below the MAPP needs to be found. When P_{PV}^{ref} exceeds the MAPP, V_{PV}^{MPP} (the PV operating voltage that corresponds to the MAPP) itself should be given out. The inherent nonlinearity in the PV's *P*–*U* curve makes the direct determination of V_{PV}^{ref} challenging. Generally, there are three categories of solutions: (1) indirect measurement methods reliant on irradiation and temperature sensors; (2) searching methods such as perturb and observe (P&O) schemes and (3) estimation methods. Considering the drawbacks of additional measurement sensors and the relatively low convergence rate of P&O methods, this paper enhances conventional estimation methods by introducing a novel characteristic curve. The details of the proposed active power control algorithm are discussed in the subsequent section.

Level 1, the innermost control loop, employs a traditional dual-loop control structure to regulate the terminal voltage of the PV array. The outer loop at level 1 controls the PV array voltage, V_{PV}, and the reactive power, while the inner loop manages the current. Under the control of level 1, when the PV array voltage, V_{PV}, equals V_{PV}^{ref}, provided by level 2, the PV output power matches the required value dictated by level 3. Notably, level 3 generates suitable power generation references according to the system frequency deviation to achieve FR capability rather than directly regulating the inverter's output frequency.

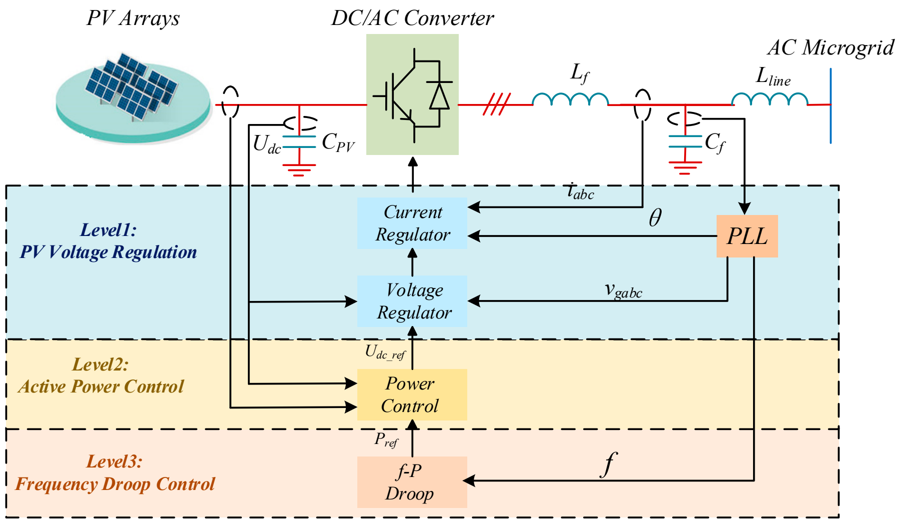

Figure 3. Structure of the PV source with proposed control system.

3. APC Algorithm Based on Characteristic Curve Fitting

3.1. The Proposed APC Algorithm

Two complex issues arise when considering flexible active power control of PV sources: (1) The *P*–*U* characteristic alters with changing ambient conditions (irradiance and temperature) changes, implying that the PV operating point (U_{PV}, P_{PV}) varies under different environmental conditions; (2) a single photovoltaic output power corresponds to two distinct operating voltages, except for the MPP. The key point for the PV power control loop can be expressed as follows:

For an arbitrary power dispatching reference, P_{ref}: If P_{ref} is lower than the MPP, then find the appropriate operating voltage (whether lower than the MPP voltage or higher, but with consistent maintenance) to equate P_{PV} with P_{ref}. While if P_{ref} exceeds MPP, then the MPP voltage should be found. In summary, the main task for PV power control is to find a PV operating voltage, U^*, that satisfies:

$$\begin{aligned} f_{pv}(U^*, G, T) = P_{ref},\ if\ P_{ref} < P_{PV}^{MPP} \\ f_{pv}(U^*, G, T) = P_{PV}^{MPP},\ if\ P_{ref} \geq P_{PV}^{MPP}, \end{aligned} \tag{3}$$

where P_{PV}^{MPP} is the real-time maximum PV power, P_{ref} is the power dispatching reference, G is the irradiance and T is the temperature.

As stated before, it is hard to obtain the function f_{pv} to solve the $f_{pv}\left(U^{*}, G, T\right) = P_{ref}$ for U^{*}. The curve fitting and interpolation iteration methods are usually used to solve these problems in numerical calculations, for example, the quadratic interpolation used in [4]. Regarding previous power curtailment algorithms in literature, the control performance is usually unsatisfactory due to sensor dependance, computation complexity or algorithm robustness. Consequently, a characteristic curve fitting-based algorithm is introduced in this section. The fundamental concept involves utilizing a curve resembling the PV's characteristic to fit the *P*–*U* curve, and then iterating until it converges on a U_{PV} value that corresponds with the given P_{PV}^{ref}. By enhancing the similarity between the real PV characteristic and the characteristic fitting curve, the robustness and convergence rate of the algorithm can be improved.

Considering two intersections with *U*-axis and the maximum point in the *P*–*U* curve of a PV array, the proposed characteristic fitting curve is given as:

$$f = \frac{x^2 + a_1 x + a_0}{b_1 x + b_0} \tag{4}$$

where a_1, a_0, b_1 and b_0 are the fitting coefficients and f is the proposed characteristic fitting curve function.

In the iterative process, only one point is sampled per iteration. Consider step k in the iterative process and assume that at least four points on the *P*–*U* curve have been sampled. The four sampling points are denoted as $\left(P_{PV}^{k-3}, V_{PV}^{k-3}\right)$, $\left(P_{PV}^{k-2}, V_{PV}^{k-2}\right)$, $\left(P_{PV}^{k-1}, V_{PV}^{k-1}\right)$ and $\left(P_{PV}^{k}, V_{PV}^{k}\right)$. The primary strategy of this method employs the fitted curve, which intersects the four sampled points, to emulate the real *P*–*U* curve and by continuous iteration, to make it converge locally to the target operating point, which is either the MPP or the power dispatch point. Once at least four sampling points are ready, the following equations are derived from Equation (4):

$$\begin{aligned}
&V_{PV}^{k} \cdot a_1 + a_0 - P_{PV}^{k} V_{PV}^{k} \cdot b_1 - P_{PV}^{k} \cdot b_0 = -{V_{PV}^{k}}^2, \\
&V_{PV}^{k-1} \cdot a_1 + a_0 - P_{PV}^{k-1} V_{PV}^{k-1} \cdot b_1 - P_{PV}^{k-1} \cdot b_0 = -{V_{PV}^{k-1}}^2, \\
&V_{PV}^{k-2} \cdot a_1 + a_0 - P_{PV}^{k-2} V_{PV}^{k-2} \cdot b_1 - P_{PV}^{k-2} \cdot b_0 = -{V_{PV}^{k-2}}^2, \\
&V_{PV}^{k-3} \cdot a_1 + a_0 - P_{PV}^{k-3} V_{PV}^{k-3} \cdot b_1 - P_{PV}^{k-3} \cdot b_0 = -{V_{VP}^{k-3}}^2.
\end{aligned} \tag{5}$$

where V_{PV}^{k} and P_{PV}^{k} with superscript k represent the PV voltage and output power in the kth iterative step, respectively. Equation (5) in then rewritten in the matrix form:

$$A \cdot s = B, \tag{6}$$

where

$$\begin{gathered}
s = \begin{bmatrix} a_1 & a_0 & b_1 & b_0 \end{bmatrix}^T, \\
B = \begin{bmatrix} -{V_{PV}^{k}}^2 & -{V_{PV}^{k-1}}^2 & -{V_{PV}^{k-2}}^2 & -{V_{PV}^{k-3}}^2 \end{bmatrix}^T, \\
A = \begin{bmatrix} V_{PV}^{k} & 1 & -P_{PV}^{k} V_{PV}^{k} & -P_{PV}^{k} \\ V_{PV}^{k-1} & 1 & -P_{PV}^{k-1} V_{PV}^{k-1} & -P_{PV}^{k-1} \\ V_{PV}^{k-2} & 1 & -P_{PV}^{k-2} V_{PV}^{k-2} & -P_{PV}^{k-2} \\ V_{PV}^{k-3} & 1 & -P_{PV}^{k-3} V_{PV}^{k-3} & -P_{PV}^{k-3} \end{bmatrix}.
\end{gathered}$$

The fitting coefficients can then be solved by $s = A^{-1} \cdot B$ or by the least square method if more than four sampling points are kept.

Once the valuables in s are obtained, substitute P_{ref} into Equation (4) and rearrange it to obtain:

$${V_{PV}^{k}}^2 + \left(a_1 - b_1 P_{ref}\right) V_{PV}^{k} + \left(a_0 - b_0 P_{ref}\right) = 0, \tag{7}$$

which can be regarded as a quadratic equation with V_{PV} being the argument.

This is defined as:

$$\Delta = \left(a_1 - b_1 P_{ref}\right)^2 - 4\left(a_0 - b_0 P_{ref}\right), \tag{8}$$

where $\Delta < 0$ means that P_{ref} has no intersections with the fitting curve, which indicates that the power dispatch reference, P_{ref}, is higher than the MPP. Under this circumstance, the PV source should operate in MPPT mode as previously discussed and the maximum point of the fitting curve is employed for the next iteration step. The maximum point can be obtained by solving the zero point of the derivative of Equation (4). The MPP voltage can be approximated as:

$$V_{pv\_ref}^{k+1} = \frac{-b_0 - \sqrt{b_0^2 - b_1(a_1 b_0 - a_0 b_1)}}{b_1}, \tag{9}$$

where $V_{pv\_ref}^{k}$ with superscript k represents the PV voltage reference for the kth iterative step. $\Delta \geq 0$ means that P_{ref} is less than or equal to the MPP and the PV source should now operate in the APC mode by regulating its output power to P_{ref}. There are two solutions to Equation (7). The uphill segment solution (denoted by UHSS) is derived as:

$$V_{pv\_ref}^{k+1} = \frac{-\left(a_1 - b_1 P_{ref}\right) - \sqrt{\Delta}}{2}, \tag{10}$$

whereas the downhill segment solution (denoted by DHSS) is derived as:

$$V_{pv\_ref}^{k+1} = \frac{-\left(a_1 - b_1 P_{ref}\right) + \sqrt{\Delta}}{2}, \tag{11}$$

In [24,25], the DHSS is regarded as a more preferrable solution for PV voltage regulation for its better control performance in many scenarios. The focus of this paper is on the versatility and simplicity of the proposed APC algorithm and the DHSS is chosen as an example. It is still worthy of noting that the proposed algorithm applies to both DHSS and UHSS and that either can be selected.

3.2. Discuss on the Properties under Large Disturbances

As previously mentioned, two potential solutions exist for when the PV system operates under the MPP: one in the uphill segment and the other in the downhill segment. Ref. [26] provides a comprehensive analysis and modeling to reveal the intrinsic characteristics of these two different operating points of a PV generation system. To ease the analysis, the operating range was divided into four regions, namely: (1) the current-source region, (2) power region I, (3) power region II and (4) the voltage-source region, as shown in Figure 4, based on their respective output characteristics. The conclusion is that power regions I and II have demonstrated superior stability and controllable performance compared to the current-source and voltage-source regions. In the current-source and voltage-source regions, the phase margin decreases significantly, which needs to be avoided by controllers to prevent system instability.

Moreover, when the reference power output is exceptionally low, the corresponding PV array voltage of the LHSS may descend below the peak voltage of the AC side of the inverter, thereby leading to inverter failure [27]. For the RHSS, such a problem will never occur. Nevertheless, it is crucial to ensure that the PV operating point does not fall into the voltage-source region. When the reference power changes abruptly, the RHSS may have faster convergence rate than that of the LHSS. This can be explained intuitively in that the downhill segment of the *P*–*U* curve is steeper than the uphill segment. To mitigate the instability caused by large disturbances, the following saturation function can be used to keep V_{PV}^{ref} within an accepted range $[V_{min}^{ref}, V_{max}^{ref}]$ (in the aforementioned power region I and power region II):

$$V_{PV}^{ref} = \begin{cases} V_{min}^{ref}, & if\ V_{PV}^{ref} < V_{min}^{ref} \\ V_{PV}^{ref}, & if\ V_{min}^{ref} < V_{PV}^{ref} < V_{max}^{ref} \\ V_{max}^{ref}, & if\ V_{PV}^{ref} > V_{max}^{ref} \end{cases} \tag{12}$$

where V_{min}^{ref} and V_{max}^{ref} are the predefined constants. The V_{max}^{ref} can be set as the maximum between the peak voltage of the AC side of the inverter and the upper boundary of the current-source region with a proper margin, whereas the V_{min}^{ref} can be set as the lower boundary of the voltage-source region to ensure the stable operation of the PV source.

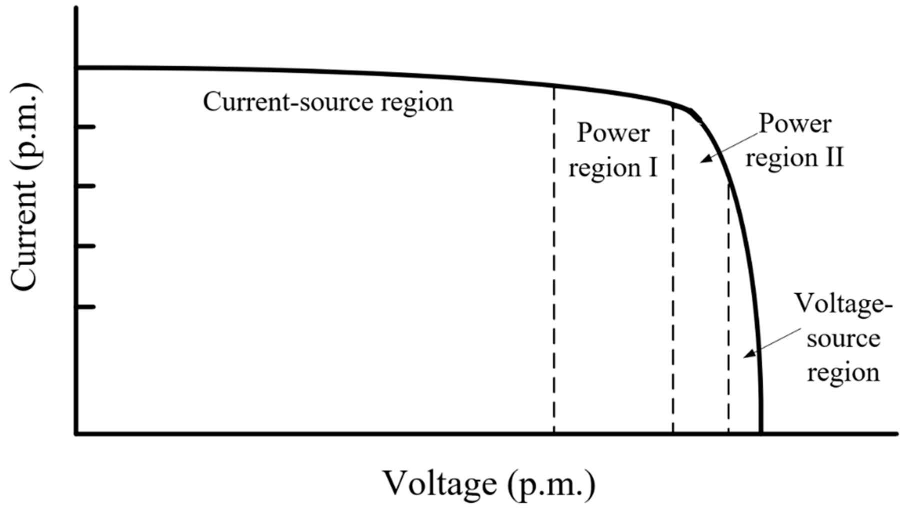

Figure 4. The I–V characteristics of a typical PV source.

4. PV Frequency Droop Control

Frequency droop control is commonly employed for primary FR and multi-source coordination (power sharing) in AC microgrids. For a traditional frequency droop type source in AC microgrids, its output current is determined based on the system frequency deviation. Traditionally, these frequency droop concepts cannot be applied to PV sources due to their lack of flexible power adjustment techniques. However, with the implementation of the APC algorithm presented in Section 3, this limitation is surmounted. A *P–f* type droop function, designed for PV frequency droop control, generates the reference PV output power in accordance with the deviation of the system frequency from its nominal value [21]:

$$P_{PV}^{ref} = P_{nom} - m \cdot \left(f_{sys} - f_{nom}\right), \tag{13}$$

where P_{PV}^{ref} is the PV generation reference, (P_{nom}, f_{nom}) is the nominal operating point, f_{sys} is the system frequency and m is the droop coefficient, which indicates the change in PV output power for per unit voltage deviation, and can be designed as:

$$m = \frac{\Delta P_{PV}}{\Delta f}, \tag{14}$$

According to Equation (13), P_{PV}^{ref} is calculated without consideration of the limit of maximum available power output, P_{PV}^{MPP}. When P_{PV}^{ref} reaches P_{PV}^{MPP}, it takes the value of P_{PV}^{MPP} and consequently loses the FR capacity. Figure 5 shows the *P–f* droop characteristics of the proposed PV frequency droop strategy. The limiting frequency, f_{lim}, is defined as the frequency at which $P_{nom} - m \cdot (f_{sys} - f_{nom})$ is equal to the real-time P_{PV}^{MPP}:

$$f_{lim} = \frac{1}{m}\left(P_{nom} - P_{PV}^{MPP}\right) + f_{nom}, \tag{15}$$

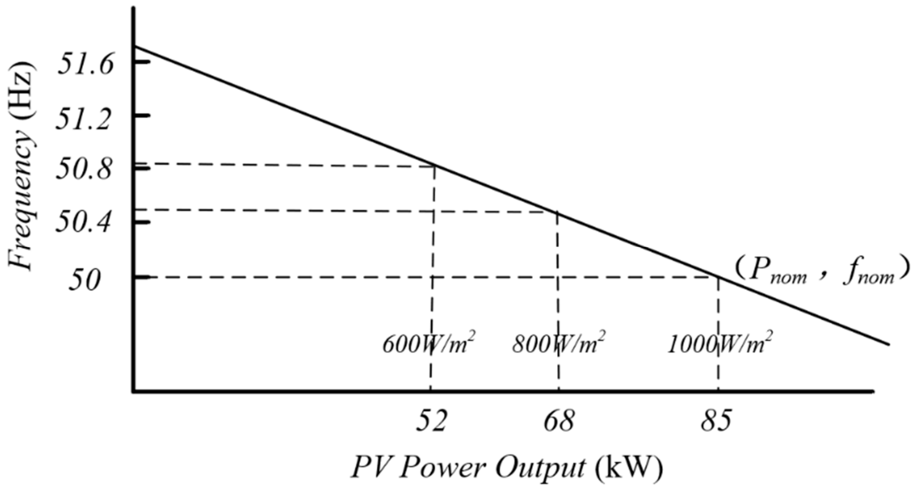

Figure 5. Steady-state characteristics of the *P*–*f* droop for PV sources.

It is apparent that the f_{lim} of the droop characteristic corresponds with P_{PV}^{MPP} and thus correlates with the irradiation and temperature. Specifically, the PV source generates P_{PV}^{MPP} if $f < f_{lim}$ while it reduces P_{PV} if $f > f_{lim}$. The proposed strategy thus adapts to various irradiation and temperature conditions. If the irradiation levels are relatively high, the FR capability of the PV source is enhanced while it is diminished under insufficient irradiance. For example, Figure 5 illustrates that at 800 W/m^2, the PV sources activate FR only when f_{sys} exceeds 50.425 Hz (which is the f_{lim} at 800 W/m^2), compared to 50 Hz at 1000 W/m^2.

In FR mode, a designated portion of the output power from PV sources is adjusted in response to system frequency deviations, based on the established *f*–*P* droop curve. This power modulation is determined by the droop coefficient, *m*, and the nominal power reference, P_{nom}. The coefficient m dictates the degree of power adjustment per frequency variation, while P_{nom} indirectly establishes the activation frequency of the FR for varying irradiance levels. Taking an 85 kW (1000 W/m^2, 25 °C) PV source as an example, the concrete FR characteristics can be found in Table 2.

Table 2. *f*–*P* droop characteristics for the 85 kWp PV source.

Irradiance (W/m^2)	Frequency to Activate FR (Hz)	m (kW/Hz)	Maximum Available Power (kW)
1000	50	40	85
900	50.2	40	77
800	50.425	40	69
700	50.625	40	60
600	50.825	40	52

Theoretically, P_{nom} can be chosen based on the system requirements. When P_{nom} is high, PV sources are unable to offer frequency regulation support at "low" (relatively low, but still higher than the nominal value) system frequency. Conversely, when P_{nom} is low, PV sources have augmented FR capability, potentially sacrificing some benefits under high irradiation. Hence, there is a trade-off between economic benefits and FR capability. For weak systems such as a small-scaled, islanded AC microgrid with high PV penetration, which inherently has a weak FR capability, more support from PV sources is necessary, thus P_{nom} should take a low-level value.

Importantly, the proposed adaptive control scheme is for efficiency promotion. In fact, if the irradiance is not sufficient, such as during shadowing time, the PV sources will try their best to harvest from the solar resource (work in MPPT mode) to enhance the system stability. The insufficient irradiation may lead to possible loss of frequency regulation capability of PV sources but the system is still governed by system-level storage or other synchronous sources. The proposed control strategy for PV sources aims to deliver frequency regulating services for the connected system, to cooperate with other synchronous sources, but not to become the only grid-forming power sources. This does not need bundled storage [28,29] in the PV generation system, but the system-level storage or synchronous sources are still needed. The service provided by PV sources may contribute to the reduction in the energy storage capacity required by the system, which may consequently reduce the installation and maintenance costs while enhancing the system operational reliability.

5. Simulation Results

A comprehensive dynamic model of an AC microgrid, composed of two PV sources, a frequency droop type energy storage and two AC loads, is established using Matlab/Simulink R2021b for simulation tests. The system configuration of the studied AC microgrid is shown in Figure 6.

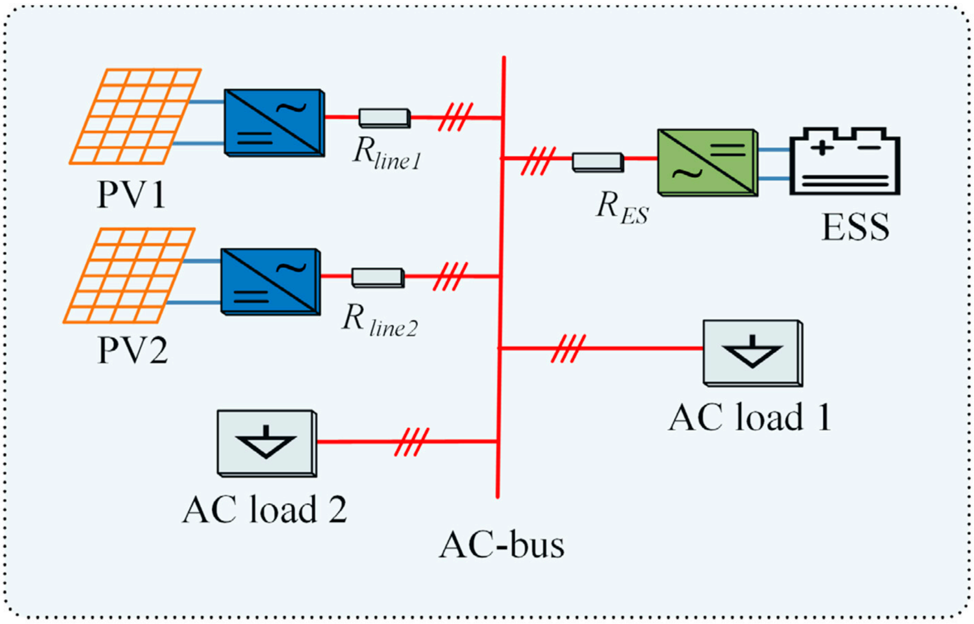

Figure 6. The AC microgrid system for simulation.

The ESS maintains the frequency and voltage of the AC microgrid. The converter of the ESS employs the conventional *P*–*f* droop control and the droop coefficient is 0.01 Hz/kW. The nominal frequency and active power are 50 Hz and 0 kW, respectively. A traditional dual loop control structure is used, with voltage and current regulator gains set to $K_{p\_v\_bat} = 1$, $K_{i\_v\_bat} = 100$ and $K_{p\_i\_bat} = 3$, $K_{i\_i\_bvat} = 200$, respectively.

Two individual PV sources exist within the studied AC microgrid to demonstrate the power sharing coordination under the proposed control strategy. Each PV source delivers a nominal output power of 85 kW at 1000 W/m^2 and 25 °C. If the PV sources use the proposed *P*–*f* droop control, the nominal frequency is set as 50 Hz with a droop coefficient of 40,000 W/Hz. However, if the PV sources use the MPPT mode, the reference power value is set at 100 kW. The sample interval for the proposed APC algorithm is 0.02 s, with the PV source's dual loop gains set to $K_{p\_v\_pv} = 0.1$, $K_{i\_v\_pv} = 1$ and $K_{p\_i\_pv} = 3$, $K_{i\_i\_pv} = 200$, respectively.

In Section 5.1, Load 1 = 85 kW and Load 2 = 85 kW while in Section 5.2, Load 1 = 70 kW and Load 2 = 85 kW. The electrical parameters of the simulation system are summarized in Table 3.

Table 3. Electrical parameters of the simulation system.

Device Name	Value
Storage	$f^* = 50$ Hz, m = 0.01 Hz/kW;
	$V^* = 311$ V, $n = 0.01$ V/kW;
	$K_{p\_v\_bat} = 1$, $K_{i\_v\_bat} = 100$;
	$K_{p\_i\_bat} = 3$, $K_{i\_i\_bvat} = 200$;
	Inductive filter: 1 mH,
	Capacitive filter: 1.5 mF;
	Line resistance : 1 mΩ;
PV1/PV2	$P_{peak} = 85$ kW;
	$f^* = 50$ Hz, m = 40 kW/Hz;
	$K_{p\_v\_pv} = 0.1$, $K_{i\_v\_pv} = 5$;
	$K_{p\_i\_pv} = 3$, $K_{i\_i\_pv} = 200$;
	Sample time interval: 0.02 s;
	Inductive filter: 1 mH,
	Capacitive filter: 1.5 mF;
	PV-side capacitor: 1.5 mF;
	Line resistance : 1 mΩ;
Loads	Section 5.1: Load 1 = 85 kW, Load 2 = 85 kW
	Section 5.2: Load 1 = 70 kW, Load 2 = 85 kW

5.1. Effect of PV Frequency Droop Control

This scenario is mainly to study the effect of PV frequency droop control. Load 2 (85 kW), accounting for approximately 50% of the system's total load, is offline at 7 s. Comparative simulation tests are conducted, comparing PV sources operating under the conventional MPPT control with those under FR control. The dynamics of the storage output powers, PV output powers and the system frequencies under different control strategies are depicted in Figures 7–9, respectively.

Prior to the disconnection of Load 2, both sets of PV sources, under different control schemes, operate in the MPPT mode for both cases. The irradiation is set as 1000 W/m^2 and the output power from each PV source is equal. After 15 s, under traditional MPPT control, all power variations in the system (Load 2) are balanced by the system storage, with charging power rising from 0 to 82 kW. The system frequency increases from 50 to over 50.8 Hz. In contrast, under the proposed frequency droop strategy, both PV sources share the power imbalance burden along with the system storage in response to a sudden load change. After 15 s, each PV source gradually reduces their output power by 17 kW and system storage only raises its charging power from 0 to 47 kW. The system frequency rises to approximately 50.5 Hz, displaying superior frequency deviation mitigation compared to traditional methodologies.

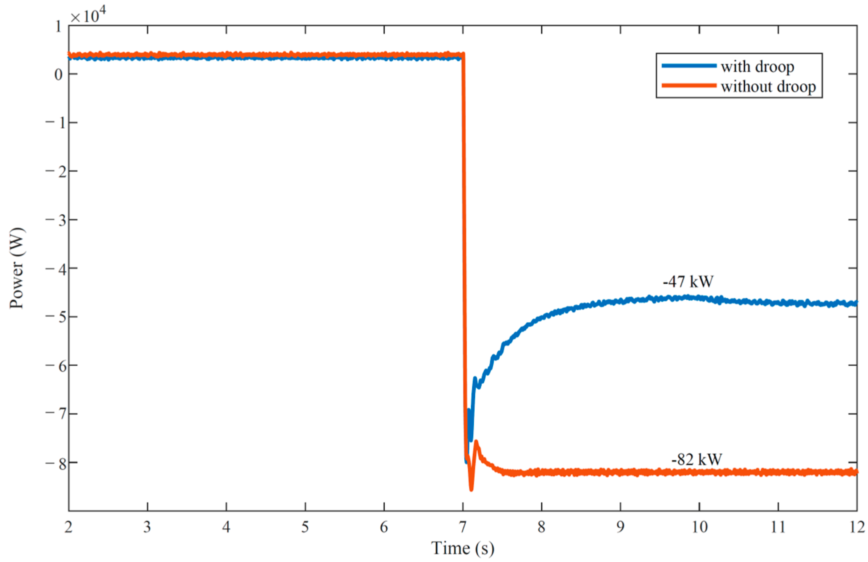

Figure 7. Storage charging power with/without droop control strategy.

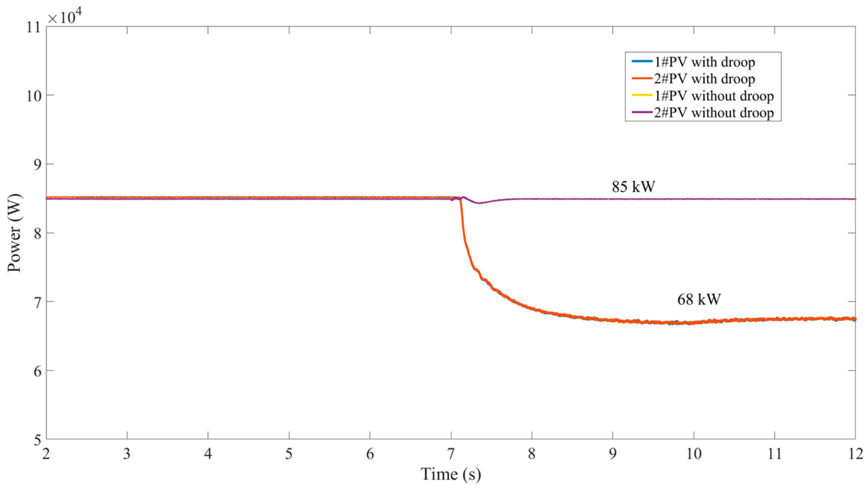

Figure 8. PV output power with/without PV droop control strategy.

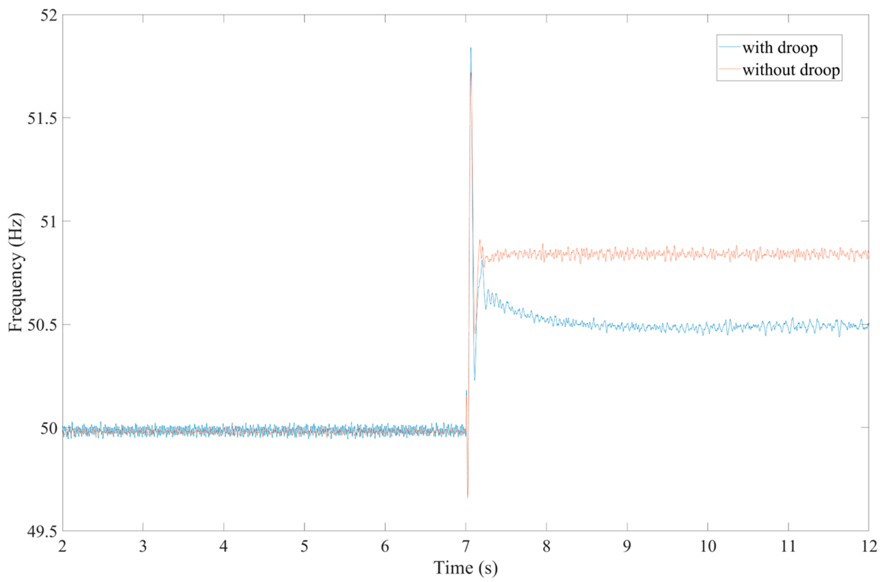

Figure 9. The system frequency with/without PV droop control strategy.

5.2. Effect of PV Different Irradiance

This scenario primarily investigates the effect of different irradiation levels. In this scenario, Load 2 (85 kW), which is 55% of the total system load in Section 5.2, is disconnected at the beginning of the test and recovers at 15 s. Similar to Section 5.1, there are still two cases, one under the MPPT scheme and the other under the proposed control strategy. Both cases are tested with three different irradiation levels (1000 W/m^2, 800 W/m^2 and 600 W/m^2, respectively). The dynamics of the storage output powers, PV output powers and the system frequencies are depicted, respectively, in Figures 10–12.

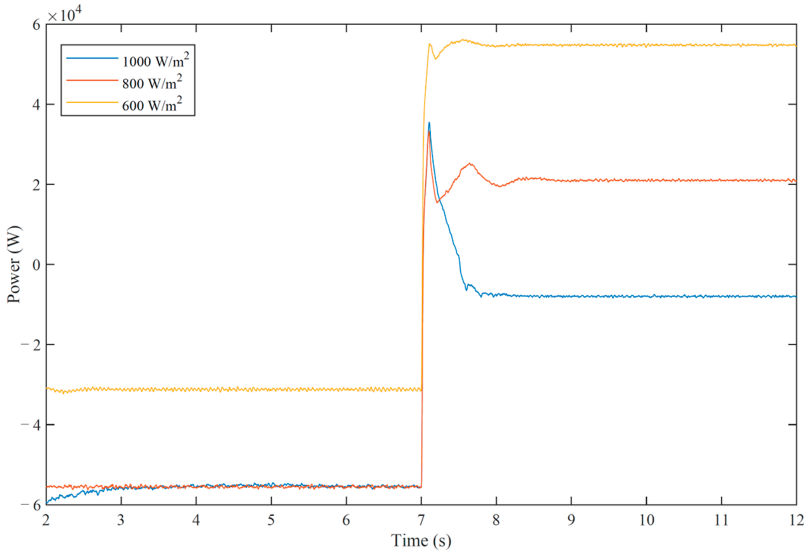

Figure 10. Storage charging power under different irradiation.

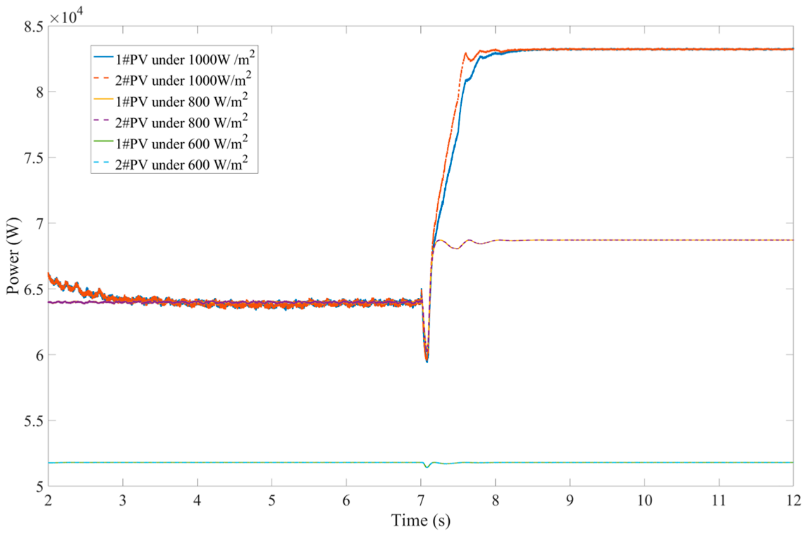

Figure 11. PV output power under different irradiation.

During the initial 15 s, the system frequency exceeds f_{lim} for 1000 W/m^2 and 800 W/m^2 and the PV sources operate in the FR mode under these two irradiation levels. However, for 600 W/m^2, as the system frequency falls below the f_{lim} for 600 W/m^2, the operation mode defaults to MPPT. Upon reconnection of Load 2, the system frequency decreases, prompting the PV sources to enhance their output power in accordance with the droop curve. As depicted in Figure 12, under low irradiation (G = 800 W/m^2 and G = 600 W/m^2 in this case), the FR capability of PV sources diminishes, causing an adaptive switch to the MPPT mode. Consequently, greater frequency drops are observed. The simulation results validate that PV sources under higher solar irradiation have stronger FR capability. If the system's original FR capability is insufficient, it is preferable to take a lower P_{nom} in order to enhance the PV FR capacity.

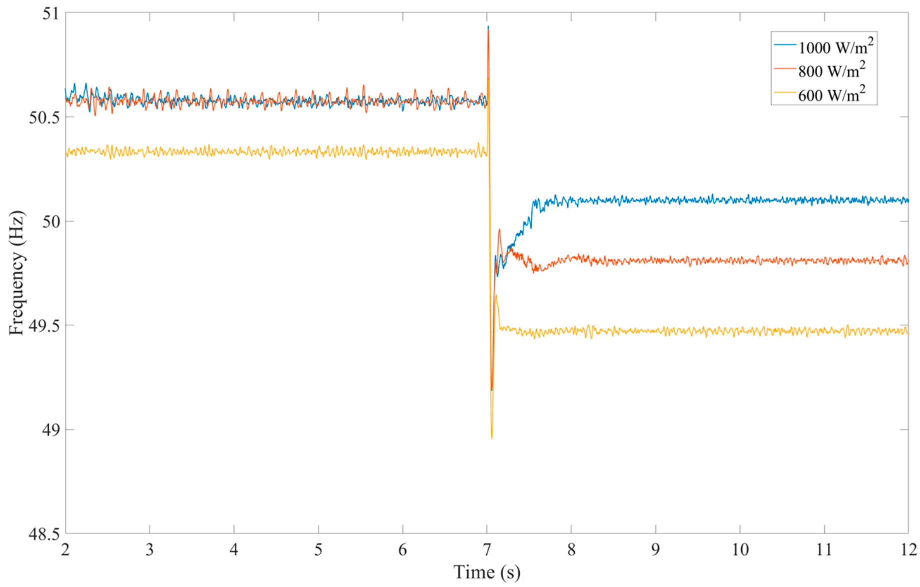

Figure 12. System frequency under different irradiation.

5.3. Test under Real Operational Scenario

In this scenario, the performance of the proposed control strategy is studied under a real operational scenario. The PV system is simulated over a 30 s period in a typical cloudy day (real irradiance data from [4,30] are used, as shown in Figure 13). The sharp variation of the solar irradiance may be because of a passing cloud, or the shade of a building. Figures 14 and 15 show the time responses of PV output power and the system frequency under both the MPPT mode and the proposed FR mode, respectively. It is proved that the PV power output can follow the change of irradiance immediately, although some frequency and power spikes can be observed when the irradiance changes too sharply. When the PV system operates in the FR mode, and if the irradiance is abundant, the FR service could significantly mitigate the frequency deviation, otherwise, the PV system adaptively switches to the MPPT mode.

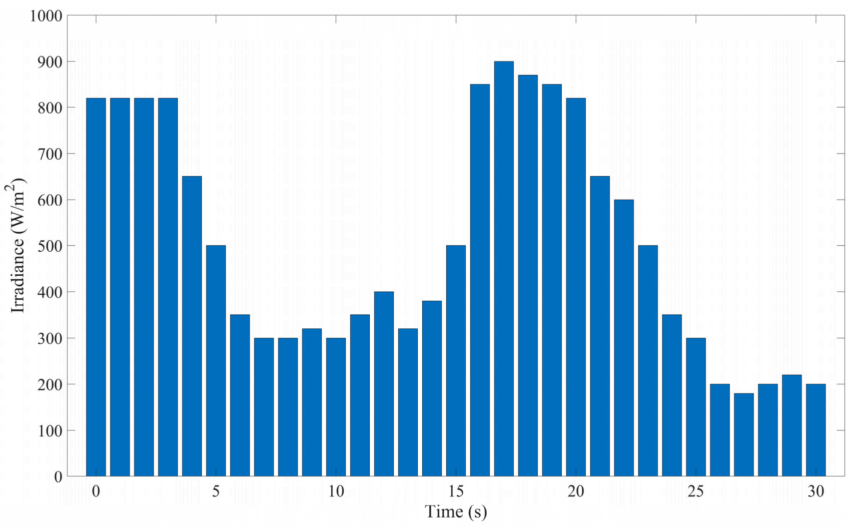

Figure 13. Variation of solar irradiance from a real scenario.

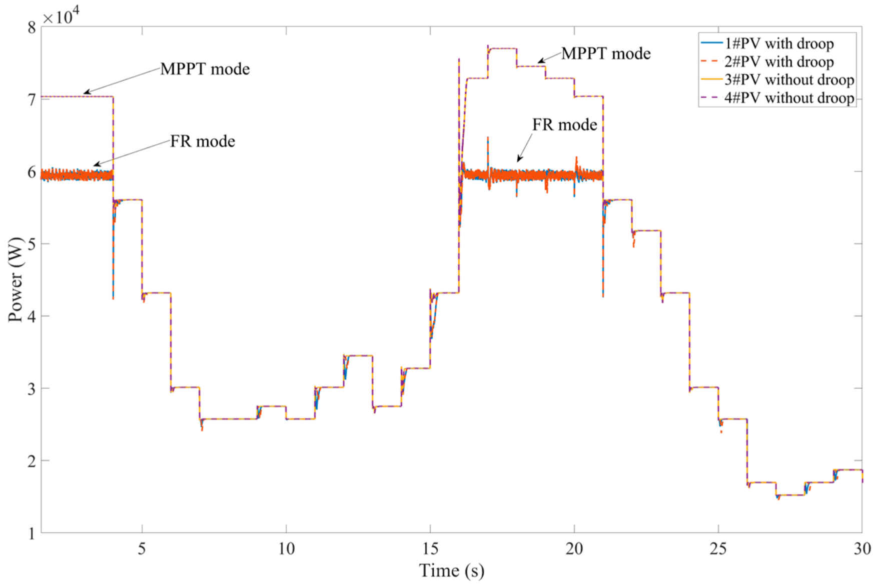

Figure 14. PV output power under different control strategies.

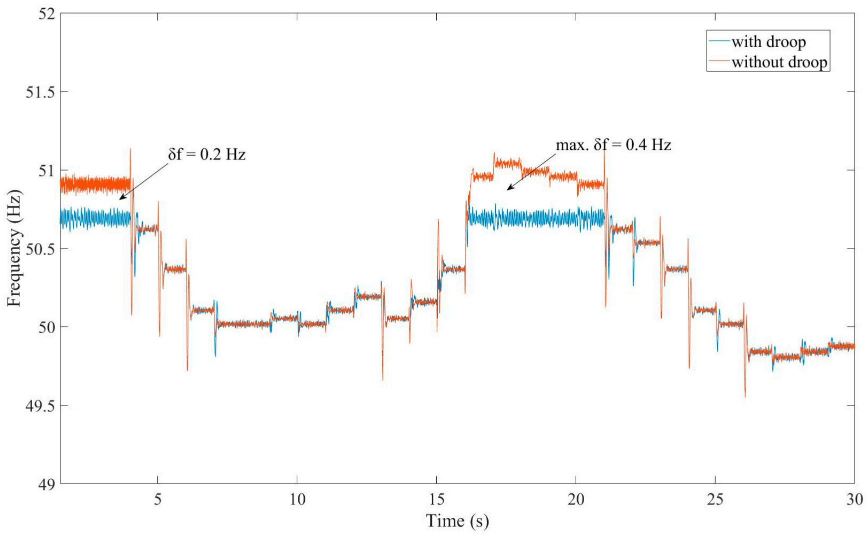

Figure 15. System frequency under different control strategies.

6. Conclusions

This study presents a unified strategy for active frequency regulation and maximum power point tracking (MPPT) pertaining to photovoltaic sources. Initially, a characteristic curve-fitting method is proposed, aimed at precisely and flexibly regulating the PV output power. The employment of a PV characteristic curve, mirroring the PV's real *P–U* curve, augments control performance and robustness. Based on the proposed active power control method, an innovative *P–f* type droop control is devised, enabling PV sources to deliver primary frequency regulation services. Under this control strategy, PV sources can adaptively participate in system frequency regulation or sustain the MPPT mode, based on the frequency and irradiation levels. Provided the irradiance is sufficient and the system frequency exceeds its nominal value, the PV source will relinquish some of its maximum available power proportionate to the frequency deviations. The frequency regulation capability attenuates with declining irradiance. Case study results substantiate that this strategy can curtail frequency deviation by approximately 25% during a 50% load shedding, with potential for further improvement via parameter settings.

The proposed control strategy is straightforward to implement as it does not require additional sensors, communication networks or complex calculations, thereby significantly reducing installation and maintenance costs and enhancing practical applicability. Nonetheless, it is imperative to consider the setting of the nominal point for PV sources to strike a balance between solar generation benefits and frequency regulation capability. Therefore, a trade-off exists between economic benefits and frequency regulation capability. Taking these considerations into account, the proposed strategy could be further refined in terms of optimal nominal point selection to boost the integration and utilization of PV sources, applicable to both distributed sources and large-scale PV plants.

Author Contributions: Conceptualization, H.C. and P.Y.; methodology, H.C.; software, J.L.; validation, Y.X., Y.Z. and P.Y.; formal analysis, W.W.; investigation, H.C.; resources, W.W.; data curation, P.Y.; writing—original draft preparation, H.C.; writing—review and editing, P.Y.; visualization, J.L.; supervision, W.W.; project administration, W.W.; funding acquisition, Y.X. All authors have read and agreed to the published version of the manuscript.

Funding: This work is supported by the Zhejiang Provincial Natural Science Foundation under grant No. LY21F030002 and National Natural Science Foundation of China (51907175).

Data Availability Statement: The data presented in this study are available on request from the corresponding author.

Conflicts of Interest: The authors declare no conflict of interest.

References

1. Rajan, R.; Fernandez, F.M.; Yang, Y. Primary Frequency Control Techniques for Large-Scale PV-Integrated Power Systems: A Review. *Renew. Sustain. Energy Rev.* **2021**, *144*, 110998. [CrossRef]
2. Alyami, S.; Wang, Y.; Wang, C.; Zhao, J.; Zhao, B. Adaptive Real Power Capping Method for Fair Overvoltage Regulation of Distribution Networks with High Penetration of PV Systems. *IEEE Trans. Smart Grid* **2014**, *5*, 2729–2738. [CrossRef]
3. Subha, R.; Himavathi, S. Active Power Control of a Photovoltaic System without Energy Storage Using Neural Network-based Estimator and Modified P&O Algorithm. *IET Gener. Transm. Distrib.* **2018**, *12*, 927–934. [CrossRef]
4. Liu, Y.; Xin, H.; Wang, Z.; Yang, T. Power Control Strategy for Photovoltaic System Based on the Newton Quadratic Interpolation. *IET Renew. Power Gener.* **2014**, *8*, 611–620. [CrossRef]
5. Seneviratne, C.; Ozansoy, C. Frequency Response Due to a Large Generator Loss with the Increasing Penetration of Wind/PV Generation—A Literature Review. *Renew. Sustain. Energy Rev.* **2016**, *57*, 659–668. [CrossRef]
6. Sangwongwanich, A.; Yang, Y.; Blaabjerg, F. High-Performance Constant Power Generation in Grid-Connected PV Systems. *IEEE Trans. Power Electron.* **2016**, *31*, 1822–1825. [CrossRef]
7. Yang, Y.; Koutroulis, E.; Sangwongwanich, A.; Blaabjerg, F. Pursuing Photovoltaic Cost-Effectiveness: Absolute Active Power Control Offers Hope in Single-Phase PV Systems. *IEEE Ind. Appl. Mag.* **2017**, *23*, 40–49. [CrossRef]
8. Varma, R.K.; Siavashi, E.; Mohan, S.; McMichael-Dennis, J. Grid Support Benefits of Solar PV Systems as STATCOM (PV-STATCOM) Through Converter Control: Grid Integration Challenges of Solar PV Power Systems. *IEEE Electrific. Mag.* **2021**, *9*, 50–61. [CrossRef]
9. Zarina, P.P.; Mishra, S.; Sekhar, P.C. Exploring Frequency Control Capability of a PV System in a Hybrid PV-Rotating Machine-without Storage System. *Int. J. Electr. Power Energy Syst.* **2014**, *60*, 258–267. [CrossRef]
10. Sangwongwanich, A.; Yang, Y.; Blaabjerg, F.; Sera, D. Delta Power Control Strategy for Multistring Grid-Connected PV Inverters. *IEEE Trans. Ind. Appl.* **2017**, *53*, 3862–3870. [CrossRef]
11. Kakimoto, N.; Takayama, S.; Satoh, H.; Nakamura, K. Power Modulation of Photovoltaic Generator for Frequency Control of Power System. *IEEE Trans. Energy Convers.* **2009**, *24*, 943–949. [CrossRef]
12. Kakimoto, N.; Satoh, H.; Takayama, S.; Nakamura, K. Ramp-Rate Control of Photovoltaic Generator with Electric Double-Layer Capacitor. *IEEE Trans. Energy Convers.* **2009**, *24*, 465–473. [CrossRef]
13. Fang, J.; Li, H.; Tang, Y.; Blaabjerg, F. Distributed Power System Virtual Inertia Implemented by Grid-Connected Power Converters. *IEEE Trans. Power Electron.* **2018**, *33*, 8488–8499. [CrossRef]
14. Batzelis, E.I.; Kampitsis, G.E.; Papathanassiou, S.A. Power Reserves Control for PV Systems with Real-Time MPP Estimation via Curve Fitting. *IEEE Trans. Sustain. Energy* **2017**, *8*, 1269–1280. [CrossRef]
15. Li, Z.; Cheng, Z.; Si, J.; Zhang, S.; Dong, L.; Li, S.; Gao, Y. Adaptive Power Point Tracking Control of PV System for Primary Frequency Regulation of AC Microgrid with High PV Integration. *IEEE Trans. Power Syst.* **2021**, *36*, 3129–3141. [CrossRef]
16. Zhong, C.; Zhou, Y.; Yan, G. Power Reserve Control with Real-Time Iterative Estimation for PV System Participation in Frequency Regulation. *Int. J. Electr. Power Energy Syst.* **2021**, *124*, 106367. [CrossRef]
17. Cai, H.; Xiang, J.; Wei, W.; Chen, M.Z.Q. V–Dp/Dv Droop Control for PV Sources in DC Microgrids. *IEEE Trans. Power Electron.* **2018**, *33*, 7708–7720. [CrossRef]
18. Cai, H.; Xiang, J.; Wei, W. Decentralized Coordination Control of Multiple Photovoltaic Sources for DC Bus Voltage Regulating and Power Sharing. *IEEE Trans. Ind. Electron.* **2018**, *65*, 5601–5610. [CrossRef]

19. Wang, Z.; Yi, H.; Zhuo, F.; Lv, N.; Ma, Z.; Wang, F.; Zhou, W.; Liang, J.; Fan, H. Active Power Control of Voltage-Controlled Photovoltaic Inverter in Supporting Islanded Microgrid without Other Energy Sources. *IEEE J. Emerg. Sel. Top. Power Electron.* **2022**, *10*, 424–435. [CrossRef]
20. Elrayyah, A.; Sozer, Y.; Elbuluk, M.E. Modeling and Control Design of Microgrid-Connected PV-Based Sources. *IEEE J. Emerg. Sel. Top. Power Electron.* **2014**, *2*, 907–919. [CrossRef]
21. Xin, H.; Liu, Y.; Wang, Z.; Gan, D.; Yang, T. A New Frequency Regulation Strategy for Photovoltaic Systems without Energy Storage. *IEEE Trans. Sustain. Energy* **2013**, *4*, 985–993. [CrossRef]
22. Gow, J.A. Development of a Model for Photovoltaic Arrays Suitable for Use in Simulation Studies of Solar Energy Conversion Systems. In Proceedings of the 6th International Conference on Power Electronics and Variable Speed Drives, Nottingham, UK, 23–25 September 1996; Volume 1996, pp. 69–74.
23. Villalva, M.G.; Gazoli, J.R.; Filho, E.R. Comprehensive Approach to Modeling and Simulation of Photovoltaic Arrays. *IEEE Trans. Power Electron.* **2009**, *24*, 1198–1208. [CrossRef]
24. Wu, D.; Tang, F.; Dragicevic, T.; Vasquez, J.C.; Guerrero, J.M. Autonomous Active Power Control for Islanded AC Microgrids with Photovoltaic Generation and Energy Storage System. *IEEE Trans. Energy Convers.* **2014**, *29*, 882–892. [CrossRef]
25. Xin, H.; Lu, Z.; Liu, Y.; Gan, D. A Center-Free Control Strategy for the Coordination of Multiple Photovoltaic Generators. *IEEE Trans. Smart Grid* **2014**, *5*, 1262–1269. [CrossRef]
26. Xiao, W.; Dunford, W.; Palmer, P.; Capel, A. Regulation of Photovoltaic Voltage. *IEEE Trans. Ind. Electron.* **2007**, *54*, 1365–1374. [CrossRef]
27. Chen, Y.; Smedley, K.M. A Cost-Effective Single-Stage Inverter with Maximum Power Point Tracking. *IEEE Trans. Power Electron.* **2004**, *19*, 1289–1294. [CrossRef]
28. Mahmood, H.; Michaelson, D.; Jiang, J. Decentralized Power Management of a PV/Battery Hybrid Unit in a Droop-Controlled Islanded Microgrid. *IEEE Trans. Power Electron.* **2015**, *30*, 7215–7229. [CrossRef]
29. Mahmood, H.; Jiang, J. Autonomous Coordination of Multiple PV/Battery Hybrid Units in Islanded Microgrids. *IEEE Trans. Smart Grid* **2018**, *9*, 6359–6368. [CrossRef]
30. Tan, Y.T.; Kirschen, D.S. Impact on the Power System of a Large Penetration of Photovoltaic Generation. In Proceedings of the 2007 IEEE Power Engineering Society General Meeting, Tampa, FL, USA, 24–28 June 2007; pp. 1–8.